



Monitoring and analytics to measure heat resilience of buildings and support retrofitting by passive cooling

Elisa López-García^a, Jesus Lizana^{b,c,**}, Antonio Serrano-Jiménez^{a,*},
Carmen Díaz-López^{a,d}, Ángela Barrios-Padura^a

^a Departamento de Construcciones Arquitectónicas I, Universidad de Sevilla, Avda. Reina Mercedes, 2, 41012, Seville, Spain

^b Department of Engineering Science, University of Oxford, Parks Road, Oxford, OX1 3PJ, United Kingdom

^c Future of Cooling Programme, Oxford Martin School, University of Oxford, Oxford, OX1 3BD, United Kingdom

^d Departamento de Ingeniería Civil, University of Granada, Campus Fuentenueva, 18071, Granada, Spain

ARTICLE INFO

Keywords:

Data science
Overheating
Data analytics
Heat resilience
Building performance analysis
Passive cooling

ABSTRACT

Designing buildings to prevent indoor overheating requires the definition of accurate procedures to measure the passive survivability of buildings and support retrofitting. This research proposes innovative diagnostic methods to audit the heat resilience of buildings using long-term monitoring data of temperature and CO₂ concentrations. The aim is to identify optimal passive cooling alternatives to retrofit the built environment through a speedy and less-disruptive assessment of the actual building performance. The approach focuses on three steps: (1) characterisation of the overheating situation of the indoor environment by a novel seasonal building overheating index (SBOI) ranging from 0 to 100%; (2) diagnosis of the indoor environment through a heat balance map that divides building performance into four thermal stages related to the positive or negative influence of total heat flux, and the ventilation and infiltration load; (3) and calculation of air change rates associated with ventilation and infiltration per thermal stage using the CO₂-based decay method. The diagnostic analytics were developed in Python and tested on three homes. The results demonstrate how the proposed approach can efficiently characterise the overheating situation of buildings, with Home 2 showing the most vulnerable scenario (SBOI > 35%). Moreover, the indicators identified the best available passive cooling opportunities concerning the reduction of solar and heat gains for Home 2, and the increase of ventilative cooling for Home 1. The research highlights the role of diagnostic analytics using real monitoring data to audit seasonal building performance beyond standard tests and simulations. The source code can be found at <https://github.com/lizanafj/analytics-to-assess-the-heat-resilience-of-buildings>.

1. Introduction

Global warming is causing an unprecedented rise in the energy demand for cooling, specifically for air conditioning (AC) [1,2]. Retrofitting existing buildings offers significant opportunities for the reduction of energy consumption and associated greenhouse emissions [3–5]. Over the last few decades, energy efficiency and the environmental impact of buildings have stood at the forefront of building directives and standards geared towards a transition to low-carbon energy [6,7]. However, recent studies indicate the need to

* Corresponding author. Departamento de Construcciones Arquitectónicas I, Universidad de Sevilla, Avda. Reina Mercedes, 2, 41012, Seville, Spain.

** Corresponding author. Department of Engineering Science, University of Oxford, Parks Road, Oxford, OX1 3PJ, United Kingdom.

E-mail addresses: jesus.lizana@eng.ox.ac.uk (J. Lizana), aserrano5@us.es (A. Serrano-Jiménez).

Nomenclature and abbreviations

AC	air conditioning
ACH	air change rate, h^{-1}
C	CO_2 concentration
c_p	specific heat, $\text{kJ/kg}\cdot\text{K}$
IAQ	indoor air quality
IoT	Internet of Things
K	first-order degradation constant, m^3/h
LCZ	local climate zone
Q	heat flux
q_v	air volume flow for ventilation and/or infiltration rate, m^3/h
RH	relative humidity, %
S	indoor emission source of CO_2 , mg/h
SBOI	seasonal building overheating index, %
t	time
T	temperature, $^{\circ}\text{C}$
V	volume, m^3

Greek letters

ρ	density, kg/m^3
--------	--------------------------

Subscripts

Ind	indoor
Inf	infiltration
Int	internal
out	outdoor
surf	surface
system	air conditioning system
t	total
ven	ventilation

look beyond energy as the sole metric of interest and consider the passive survivability of buildings (without AC systems). Potential trade-offs have been identified when synergies between passive survivability and energy performance are not considered [8,9]. It has been demonstrated how improving insulation and infiltration can reduce overheating in well-designed buildings, but can increase overheating in others if ventilation is inadequately addressed [10]. This decreases the heat resilience capacity of building stock, thereby affecting citizens' quality of life, especially in situations of fuel poverty [11]. In this context, the definition of accurate analytical procedures is required for the selection of the best available technologies to support retrofitting based on the real needs of buildings [12,13].

The Internet of Things (IoT) enables the connection and exchange of data with buildings, devices, and systems over different communication networks [14]. Many innovative applications have been proposed in the built environment to help transform the building stock into a smart, efficient, and secure environment [15]. These applications can be classified as automation, intelligent energy management systems, and health and safety [15]. Additionally, IoT sensors can also enable a helpful new data source to delve into indoor building performance, by going beyond traditional audits to support the retrofitting of buildings [16]. The combination of IoT with data science to analyse the time series of real building operational data can help identify specific flaws in the built environment [17]. This approach has been widely applied to evaluate indoor air quality (IAQ) and energy consumption in buildings.

Regarding the IAQ trends, previous studies show high CO_2 concentrations and indoor air pollutants to be due to inadequate ventilation [18], above all during extreme heat events caused by reduced window-opening periods [19]. Inadequately ventilated bedrooms were highlighted as responsible for approximately 60% of children's total inhaled dose of air pollutants [20]. Other studies have shown the efficacy of natural and mechanical ventilation systems with low and high ventilation rates to improve IAQ [21], thereby highlighting the positive effect of suitable natural ventilation [22,23].

On the other hand, the analysis of energy data has been widely utilised to identify retrofitting measures for high-performance buildings [16]. Previous studies were focused on: comparing the relationship between energy demand and energy use to identify potential energy savings [24]; automatic control using IoT-based monitored data to improve building efficiency, reduce energy demands, and enhance the user's experience within the building [25]; and on further data analytics to help transform the building into a nearly zero-energy building (nZEB) [26].

Despite all these contributions, most existing approaches are based on IAQ or energy targets, not existing analytical methods and indicators for the assessment of passive building performance. There is a potential research gap in IoT-based data analysis procedures

for the understanding of the full potential of this approach in supporting the decision-making process regarding building retrofitting for the improvement of heat resilience or passive survivability of the built environment [15].

This research defines an innovative set of analytics to assess the indoor overheating of buildings using real long-term monitoring data obtained through indoor and outdoor IoT sensors. The aim is to determine heat vulnerabilities in buildings and identify optimal passive cooling opportunities to retrofit the built environment through a swift and less-disruptive assessment of the real operational phase. The diagnostic analytics are based on three methods using indoor and outdoor temperatures and CO₂ concentrations. First, the overheating situation in the indoor environment is characterised by a novel seasonal building overheating index (SBOI) ranging from 0% to 100%. Second, the indoor environment is diagnosed through a heat balance map that divides building performance into four thermal stages related to the positive or negative influence of total heat flux and to the ventilation and infiltration load. Third, the air changes (ACH, h⁻¹) associated with ventilation and infiltration per thermal stage are calculated using the CO₂-based decay method. The approach was iteratively developed, tested, and validated using monitored data in three residential homes, characterised by different construction periods, geometry, orientation, ventilation systems, building standards, and operating conditions. Two main research contributions are provided in this work:

- Three innovative diagnostic analytic methods to audit seasonal passive cooling building performance using long-term monitoring data were developed and validated using Python code. The novelty is based on the use of real monitoring data (indoor and outdoor temperature and CO₂ concentrations) to assess indoor overheating situations and identify optimal passive cooling opportunities in buildings through a speedy and less-disruptive assessment of the real building performance. The source code can be found at <https://github.com/lizana/fj/analytics-to-assess-the-heat-resilience-of-buildings>.
- Additionally, specific building configurations and properties that promote indoor overheating are identified by using these diagnostic analytics. These key characteristics should be prioritised in the retrofitting actions of building stock and in the support of the implementation of additional requirements in future retrofitting regulations and guidelines.

The paper is structured as follows. First, the data to validate the analytical approach is described in Section 2.1. Second, the diagnostic analytics to audit passive building performance are detailed in Section 2.2. Third, the results are presented and discussed in two sections: a descriptive analysis of data is provided in Section 3.1, and the results of the diagnostic analytics are detailed in Section 3.2. This section is divided into the overheating situation per case study, the evaluation of thermal stages, and the characterisation of ventilation and infiltration rates. Finally, the potential practical implications of the analytical approach are discussed, and the main conclusions are drawn.

2. Data and methods

This section defines the data used and explains the set of diagnostic analytics developed to evaluate the overheating situation of the built environment and to support building retrofitting. The proposed IoT workflow is divided into four stages, as illustrated in Fig. 1: perception layer (data generation), network layer (data acquisition), processing layer (data storage and data analytics), and application layer (data visualization). The data employed is based on long-term monitoring data of indoor and outdoor temperatures and CO₂ concentrations using IoT-based sensors, as detailed in Section 2.1. The diagnostic analytics are described in Section 2.2. The methods were developed in a python script. The source code and the monitored datasets are published under the MIT licence on GitHub (<https://github.com/lizana/fj/analytics-to-assess-the-heat-resilience-of-buildings>) together with additional documentation and tutorials.

2.1. Data

2.1.1. Monitoring campaign

Three different housing typologies in southern Europe were monitored from 01 June 2021 to 31 August 2021. They consist of three homes in multi-family buildings in Seville (Spain). They are representative of three different building situations: a slightly insulated home with AC (Home 1), a poorly insulated home without AC (Home 2) and a well-designed home following the current building code (Home 3). The homes are also located in three different urban contexts (Fig. 2, red dots) according to the urban climate classification system proposed by Stewart & Oke [27]. Home 1 and Home 3 are open midrise areas (local climate zone 5, LCZ-5), with Home 3

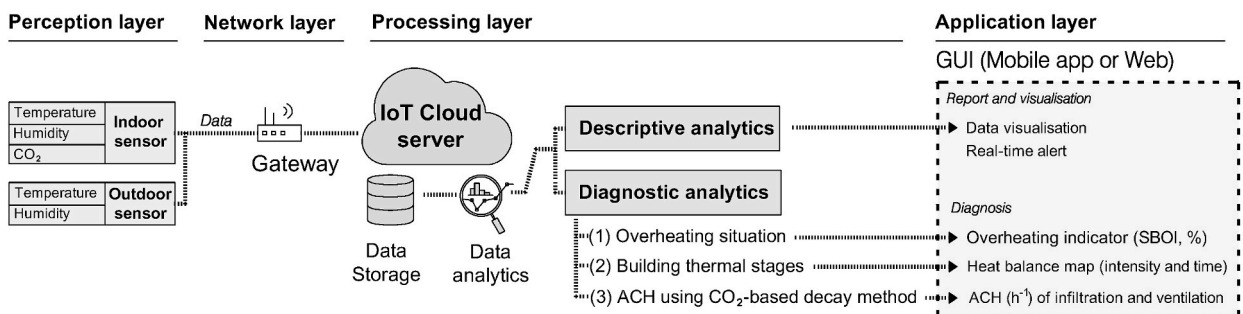


Fig. 1. Analytic workflow showing the interrelations between input data and output indicators for building diagnosis.

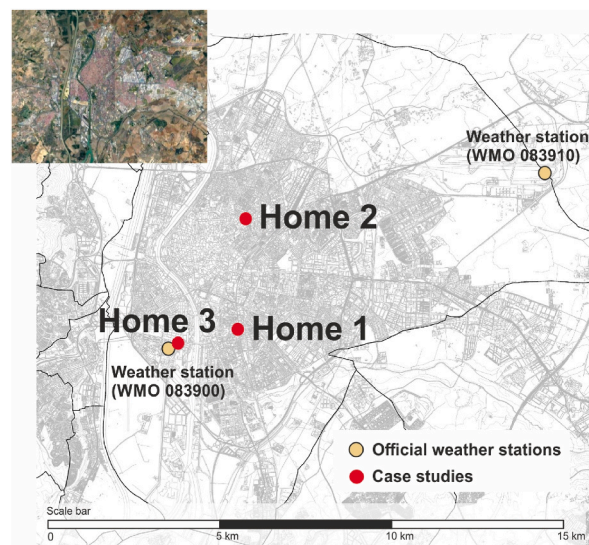


Fig. 2. Aerial image and location of selected case studies in Seville (Spain).

located in a suburban area. Home 1 is close to the city centre, characterised by a compact midrise area (LCZ-2).

Temperature (T), relative humidity (RH), and carbon dioxide (CO_2) concentrations in homes were monitored using IoT-based devices (model TESTO 160 IAQ using the TESTO Museum platform). Sensors were located in bedrooms 1.0 m above the floor and separated more than 1.5 m from the openings. The logging interval was defined as being every 15 min, and quality control procedures

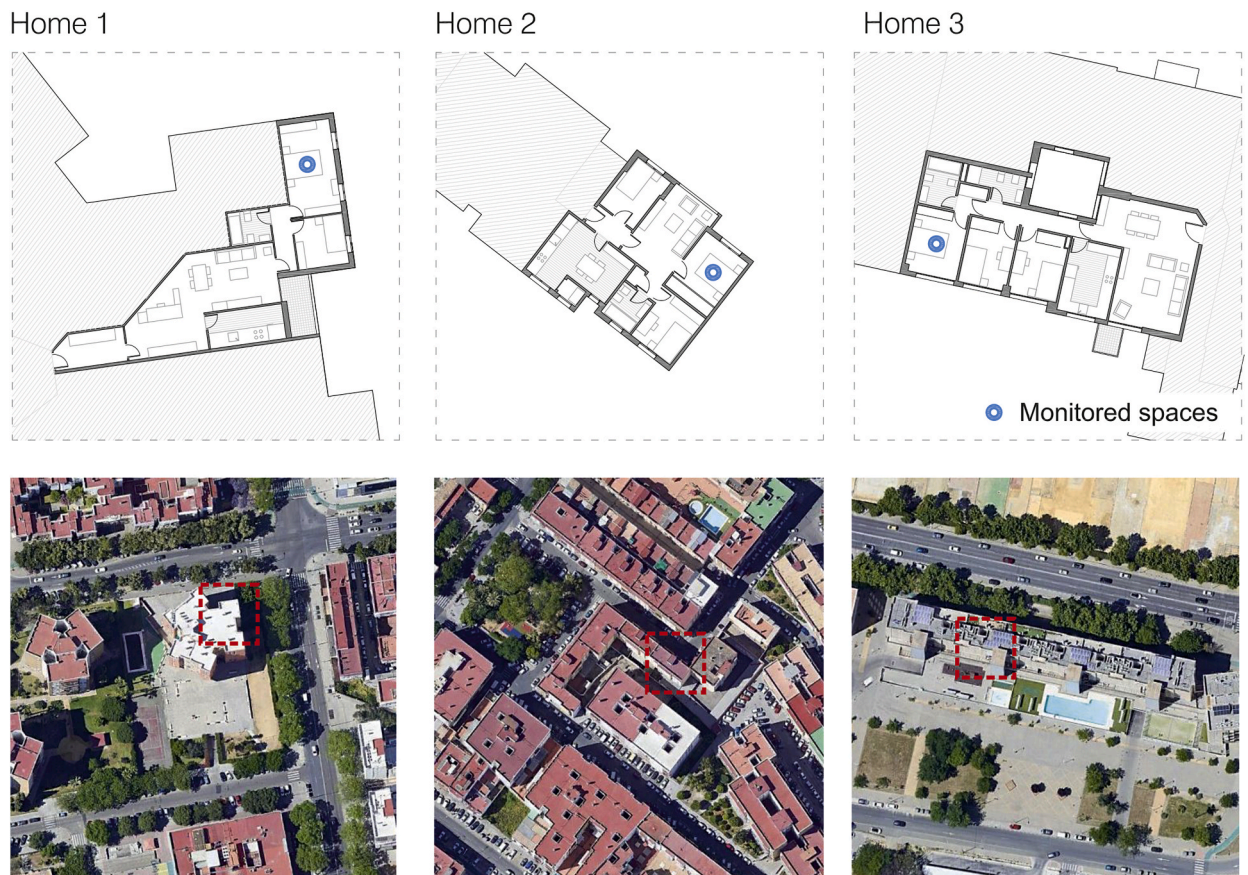


Fig. 3. Floor plan and urban context of selected case studies.

were applied. The sensors have an accuracy of ± 0.5 °C, $\pm 3\%$, and ± 50 ppm for T, RH, and CO₂, respectively. Moreover, weather data from the nearest official weather stations (National Meteorological Agency in Spain) in Seville (WMO 083900 and WMO 083910) were used, which are located in rural/urban areas (Fig. 2, brown dots) [28].

2.1.2. Characterisation of monitored indoor environments

The geometry and orientation of the three homes are illustrated in Fig. 3. Furthermore, their general characteristics, building envelope properties, ventilation systems, AC units, and user behaviour patterns are summarised in Table 1.

Home 1 is located on the top floor of a multi-family building. This was built following the first national standard that fixed minimum thermal requirements for building envelopes (NBE-CT-79). This case comprises 29% of the Spanish residential housing stock [29]. In addition, its windows have recently been replaced with a double-glazing system. Its main orientation is east, with single-sided ventilation. This case study has an AC system, a split unit, operating partially at night during the monitored period.

Home 2 is located on the top floor of a multi-family building. It was built before the first thermal regulation of buildings in Spain (NBE-CT-79), and presents low insulation properties. This case involves 42% of the Spanish residential housing stock [29]. The main orientation of the openings is northeast, with cross ventilation.

Home 3 is located on an intermediate floor of a multi-family block. This case follows the current building code, and is well-insulated. This situation represents approximately 13% of Spanish residential building stock [29]. Its main orientation is south, and the space is well-ventilated thanks to an inner courtyard, which allows cross ventilation. It is located in a suburban area, with no influence of urban heat island and with no obstacles to outdoor airflow. This case has a centralised AC unit, which was not used during the monitored period.

2.2. Data analytics to characterise the passive performance of buildings

The proposed data diagnostic analytics are divided into three methods: the analysis of the indoor overheating situation of buildings through a new indicator known as the seasonal building overheating index (SBOI, %) (Section 2.2.1); the identification of potential passive cooling opportunities through the analysis of four building thermal stages related to the positive or negative influence of total heat flux, and through the ventilation and infiltration load (Section 2.2.2); and the calculation of ACH per thermal stage using the CO₂-based decay method (Section 2.2.3).

These indicators require input data of indoor and outdoor temperatures and CO₂ concentrations exclusively based on the passive thermal performance of the building. Passive thermal performance refers to heat transfer between a building and its surroundings, mainly without AC systems.

2.2.1. Analysis of the overheating situation

Firstly, an indicator to measure the overheating situation of the indoor environment is proposed. It is based on the temperature difference between outdoor and indoor environments ($T_{out,i} - T_{in,i}$). The proposed indicator, named Seasonal Building Overheating Index (SBOI, %), ranges from 0 to 100%, and it is calculated in accordance with Eq. (1). It provides a measurable parameter that describes the appropriate or inappropriate passive building performance.

$$SBOI(\%) = \frac{\sum T_{out,i} - T_{in,i} \text{ if } < 0}{\left(\sum |T_{out,i} - T_{in,i}| / 2 \right)} - 1 \quad \text{Eq. (1)}$$

Table 1
Characteristics of selected case studies.

Characteristics	Home 1	Home 2	Home 3
General description	Slightly insulated home with AC	Poorly insulated home without AC	Well-designed home
General characteristics			
Construction year	1986	1973	2010
Area	81 m ²	68 m ²	108 m ²
Floor	8th floor (top floor)	4th floor (top floor)	3rd floor (intermediate floor)
Main orientation of windows	East	Northeast	South
Building regulation	NBE-CT-79	MV-1957	CTE-2006
Urban morphology	open midrise (LCZ-5)	compact midrise (LCZ-2)	open midrise (LCZ-5)
Building envelope			
Windows	U-value: 3.8 W/m ² ·K	U-value: 4.1 W/m ² ·K	U-value: 2.2 W/m ² ·K
Façade	U-value: 0.8 W/m ² ·K	U-value: 1.4 W/m ² ·K	U-value: 0.5 W/m ² ·K
Roof	U-value: 1.1 W/m ² ·K	U-value: 1.6 W/m ² ·K	–
Ventilation			
Natural ventilation	single-sided ventilation	cross ventilation	cross ventilation with an inner courtyard
Mechanical ventilation	yes (in bathrooms)	No	Yes (in bathrooms)
Systems			
Fan	No	Ceiling fan	No
AC unit	split AC unit	No	Centralised AC system
User behaviour			
Night ventilation	No	Yes	Yes
Use of AC	Night periods (0:00–8:00)	No	No

Fig. 4 shows two typical indoor and outdoor temperature curves on a hot day: (a) for a well-designed building; and (b) for an overheated building.

On the one hand, in a well-designed building scenario (Fig. 4a), the SBOI should be closer to 0%, and show an indoor environment thermally well-balanced, with similar red and blue areas. In this case, it is possible to assume that the sum of positive and negative heat fluxes, as defined in Eq. (2), tends towards zero.

On the other hand, in an overheated indoor environment (Fig. 4b), SBOI results in a higher value ranging from 10% to 100%. It is associated with high heat fluxes related to internal, solar or ventilation heat gains, combined with a low heat dissipation rate. The following overheating thresholds, illustrated in Fig. 4b, are proposed:

- SBOI >10%: slightly overheated indoor environment.
- SBOI >25%: overheated indoor environment.
- SBOI >50%: extremely overheated indoor environment.
- And SBOI ≈100%: tremendously overheated indoor environment, where the indoor temperature is always higher than outside.

2.2.2. Analysis of building thermal stages

Secondly, the thermal performance of the building is analysed through four thermal stages related to the positive or negative influence of total heat flux, and the ventilation and infiltration load. These stages can be labelled according to the three main action groups for the passive conditioning of buildings [30,31], namely heat modulation (Stage 1), solar and heat gains (Stages 2 and 3) and heat dissipation (Stage 4). The thermodynamics describing these thermal stages of buildings are given in detail below.

The most influential factors on passive performance in a hot climate are geometry and orientation, thermal properties of building materials, solar properties of openings and opaque envelope, internal gains (occupancy, lighting, and appliances), ventilation, air infiltration, and internal heat capacity (or thermal mass). The total heat balance of an indoor air node (Q_t) concerning all these parameters can be defined by Eq. (2) [32,33], where heat dissipation is mainly associated with the negative heat fluxes of \dot{Q}_{surf_i} and $\dot{Q}_{ven+infi}$.

$$\pm \dot{Q}_t = \pm \dot{Q}_{surf_i} + \dot{Q}_{int_i} + \dot{Q}_{solar_i} \pm \dot{Q}_{ven+infi} - \dot{Q}_{system_i} \quad \text{Eq.(2)}$$

where:

$\pm \dot{Q}_t$: total heat flux of indoor air node (KJ/h).

\dot{Q}_{surf} : convective gain from indoor opaque surfaces and windows. This involves the heat transfer processes with the outdoor environment and the heat absorbed and/or released by the surfaces as a result of internal, solar, and radiative loads.

$\dot{Q}_{inf+vent}$: infiltration and natural ventilation gains.

\dot{Q}_{int} : internal convective gains (occupants, lighting, and appliances).

\dot{Q}_{solar} : fraction of solar radiation through the window directly to internal air (convective gain).

\dot{Q}_{system} : the heat input from a system for cooling/heating.

Assuming a building heat balance in free-running conditions, where AC systems are not used or are used sporadically ($\dot{Q}_{system_i} \approx 0$), the passive building performance can be categorised into four thermal stages related to the positive or negative influence of total heat flux ($\pm \dot{Q}_t$), and the positive or negative influence of ventilation and infiltration load ($\pm \dot{Q}_{ven+infi}$). Moreover, given that heat dissipation loads can be related to only \dot{Q}_{surf_i} or $\dot{Q}_{ven+infi}$, it is possible to deduce the intensity of other loads that influence building performance per

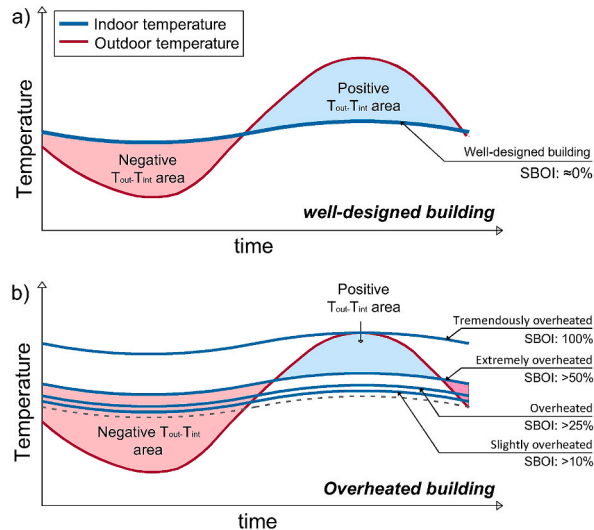


Fig. 4. Typical indoor and outdoor temperature curves on a hot day for (a) a well-designed building, and (b) an overheated building.

thermal stage as follows:

- **Stage 1. Heat modulation.** This stage refers to the building period with a total negative heat flux ($-Q_t$, < 0) mainly associated with the building thermal mass ($-Q_{surf_i}$), as defined by Eq. (3). During this period, indoor building surfaces absorb heat gains and passively cool the indoor environment even with a positive ventilation load ($+Q_{ven+inf_i}$) due to the higher outdoor temperature. This technique depends on the thermal mass of the building structure to store and remove heat gains.

$$\begin{aligned} Q_t < 0 \\ -Q_{surf_i} + Q_{int_i} + Q_{solar_i} + Q_{ven+inf_i} - Q_{system_i} < 0 \\ +Q_{int_i} + Q_{solar_i} + Q_{ven+inf_i} < Q_{surf_i} + Q_{system_i} \end{aligned} \quad \text{Eq.(3)}$$

- **Stage 2. Solar and heat gains 1/2.** This stage consists of a positive temperature gradient ($+Q_t$) where the building is heating up with the higher outside temperature ($+Q_{ven+inf_i}$). High thermal gradients in this stage may indicate low insulation levels (affecting $+Q_{surf_i}$), high solar gains through windows or opaque surfaces ($+Q_{surf_i} + Q_{solar_i}$), high internal heat gains ($+Q_{int_i}$) and/or high ventilation and infiltration rates ($+Q_{ven+inf_i}$), as shown in Eq. (4).

$$\begin{aligned} Q_t > 0 \\ \pm Q_{surf_i} + Q_{int_i} + Q_{solar_i} + Q_{ven+inf_i} - Q_{system_i} > 0 \\ \pm Q_{surf_i} + Q_{int_i} + Q_{solar_i} + Q_{ven+inf_i} > Q_{system_i} \end{aligned} \quad \text{Eq.(4)}$$

- **Stage 3. Solar and heat gains 2/2.** This period is associated with building hours in which the indoor air node is heating up (positive temperature gradient, $+Q_t$) even with a lower outside temperature, or in other words, a negative ventilation load ($-Q_{ven+inf_i}$), as described in Eq. (5). This situation may be directly associated with poorly ventilated scenarios (with a low ACH value), low quality of the thermal building envelope (high $+Q_{surf_i}$ rate), and/or high internal heat gains ($+Q_{int_i}$), and may indicate a major opportunity for ventilative cooling.

$$\begin{aligned} Q_t > 0 \\ \pm Q_{surf_i} + Q_{int_i} + Q_{solar_i} - Q_{ven+inf_i} - Q_{system_i} > 0 \\ \pm Q_{surf_i} + Q_{int_i} > Q_{ven+inf_i} + Q_{system_i} \end{aligned} \quad \text{Eq.(5)}$$

- **Stage 4. Heat dissipation.** This final stage illustrates heat rejection from the building with the support of a suitable environmental heat sink at a lower temperature. In this case, existing cooling periods with a total negative heat flux ($-Q_t$) are mainly associated with ventilative cooling ($-Q_{ven+inf_i}$), as detailed in Eq. (6).

$$\begin{aligned} Q_t < 0 \\ +Q_{surf_i} + Q_{int_i} + Q_{solar_i} - Q_{ven+inf_i} - Q_{system_i} < 0 \\ +Q_{surf_i} + Q_{int_i} < Q_{ven+inf_i} + Q_{system_i} \end{aligned} \quad \text{Eq.(6)}$$

With this framework, by using real long-term monitoring data of indoor and outdoor temperatures (T , in $^{\circ}\text{C}$), it is possible to characterise each measured value of the building in its corresponding thermal stage.

It is possible to affirm that Q_t is positive when the indoor temperature increases (positive gradient) and negative when it decreases (negative gradient). Thus, the derivative of indoor temperature, whose value provides the temperature gradient over time ($^{\circ}\text{C}/\text{h}$), represents the positive or negative rate of total heat flux (Q_t) in the indoor environment [34].

Moreover, by comparing the difference between outdoor and indoor temperatures ($T_{out}-T_{ind}$), it is possible to ascertain the positive or negative influence of $Q_{ven+inf_i}$ in the heat balance. The heat flow related to ventilation and infiltration load ($Q_{ven+inf_i}$) can be given by Eq. (7) [32,33], whose sign and intensity are mainly associated with the outdoor-indoor temperature difference ($T_{out_i}-T_{ind_i}$) and the air change rate (ACH , h^{-1}).

$$\pm Q_{ven+inf_i} = q_{vi} \cdot \rho \cdot c_p (T_{out_i} - T_{ind_i}) = \text{ACH}_i \cdot V \cdot \rho \cdot c_p (T_{out_i} - T_{ind_i}) \quad \text{Eq.(7)}$$

where:

q_{vi} : air volume flow for ventilation and/or infiltration rate (m^3/h).
 ρ : density of air ($1.2 \text{ kg}/\text{m}^3$).

c_p : specific heat of the air (1.0 kJ/kg·K).

$T_{out,i}$: outdoor temperature (supply temperature for ventilation and infiltration).

$T_{int,i}$: indoor temperature.

ACH_i : air change rate (h^{-1}).

V : volume of indoor space (m^3).

As a result, with these two parameters, $T_{out}-T_{ind}$ and indoor temperature gradient ($^{\circ}\text{C}/\text{h}$), it is possible to calculate the percentage of time in which the heat flow of the building operates in every previously defined thermal stage. Moreover, a heat balance map showing intensities of building performance per stage can be obtained. An example of the building heat balance map is illustrated in Fig. 5, and Table 2 summarises the indicators obtained related to the percentage of time per thermal stage.

The building heat balance map in Fig. 5 helps visualise and qualify the different heat loads affecting passive building performance. Stage 1 mainly shows cooling periods due to the thermal mass of the building (or sporadic AC operation). Stage 2 illustrates the temperature increasing as a result of solar and heat gains. Stage 3 illustrates the temperature increasing despite the lower outdoor temperature. In this stage, heat fluxes of the building surface and internal heat gains are predominant. And Stage 4 is associated with cooling periods mainly due to ventilative cooling (or sporadic AC operation). This illustration, in which every point is a monitored value over time, along with the quantification of time per stage, summarised in Table 2 (%), provides measurable indicators to identify heat vulnerabilities and highlight passive cooling opportunities.

2.2.3. Analysis of ACH through the CO_2 -based decay method

The CO_2 -based ventilation analysis provides information on the operating conditions of the building related to ventilation and air infiltration rates per stage, which are directly associated with user behaviour and building design. These results can support the decision-making process in identifying additional measures or user behaviour strategies related to ventilation to improve passive building performance.

In this analysis, monitored data relating to indoor CO_2 concentrations in the indoor environment is employed to calculate the air change rate (ACH, h^{-1}) related to ventilation and air infiltration through the CO_2 -based decay method [35–37]. This method calculates the ventilation rates associated with infiltration, and natural and mechanical ventilation in buildings, since ventilation is the only significant process for carbon dioxide removal in the indoor environment [36,37]. For a contaminant of interest, in this case CO_2 , the governing equation for this model is defined in Eq. (8), which calculates the change of any indoor pollutant based on its concentration:

$$V \frac{dC}{dt} = \text{inflows} - \text{outflows} + \text{sources} - \text{degradation} \quad \text{Eq.(8)}$$

$$V \frac{dC}{dt} = q_{v,\text{inlet}} \cdot C_{out} - q_{v,\text{outlet}} \cdot C_{ind} + S - K \cdot C_{ind}$$

where:

V : room volume (m^3).

q_v : airflow inlet/outlet of the building (m^3/h).

C_{out} : outdoor CO_2 concentration (mg/m^3).

C_{ind} : indoor CO_2 concentration (mg/m^3).

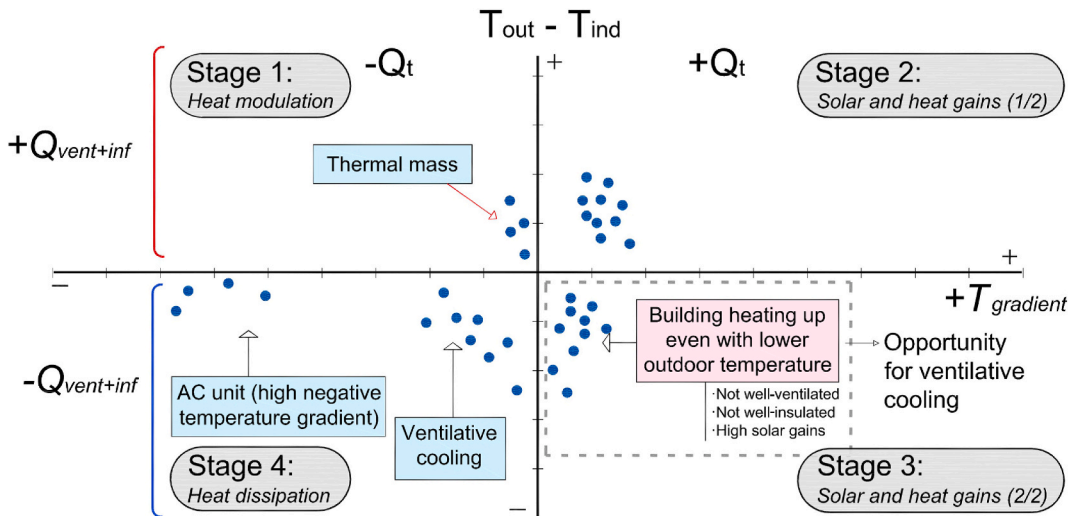


Fig. 5. Example of a heat balance map to audit passive building performance through four stages. Stage 1: heat modulation; Stage 2: solar and heat gains (1/2); Stage 3: solar and heat gains (2/2); Stage 4: heat dissipation.

Table 2

Summary of indicators provided by the analysis of building thermal stages. Each building stage is characterised by the percentage of the time.

	Negative total heat flux (− Q_{ti})	Positive total heat flux (+ Q_{ti})
+ $Q_{\text{ven+inf}_i}$ (Mostly daytime)	Percentage of time in Stage 1 (%)	Percentage of time in Stage 2 (%)
− $Q_{\text{ven+inf}_i}$ (Mostly night-time)	Percentage of time in Stage 4 (%)	Percentage of time in Stage 3 (%)

S: indoor emission source of CO₂ (mg/h).

K: first-order degradation constant (m³/h).

In the case where there is neither degradation nor an indoor source of CO₂, and by solving Eq. (8) through integration, the expression can be rewritten to obtain the Q/V value, and hence the air change rate (ACH, h^{−1}), according to Eq. (9) becomes:

$$ACH_t = \frac{1}{t} \ln \frac{C_{\text{ind},t=0} - C_{\text{out}}}{C_{\text{ind},t} - C_{\text{out}}} \quad \text{Eq.(9)}$$

where:

ACH: air change rate (h^{−1}) at time t.

$C_{\text{ind},t=0}$: indoor CO₂ concentration (ppm) at time t = 0.

$C_{\text{ind},t}$: indoor CO₂ concentration (ppm) at time t.

C_{out} : outdoor CO₂ concentration (400–500 ppm).

This approach enables the real-time oscillation of ACH in buildings to be evaluated according to its urban location, orientation, geometry, whether it is single-sided or cross-ventilation, and whether it has a mechanical ventilation system or natural ventilation habits. According to laboratory tests, this method shows an accuracy of ±10% [36] and has been widely applied to evaluate ventilation ranges in buildings [22,35,37]. However, this method has two main limitations when applied to a real environment. ACHs should be obtained from CO₂ concentration decay curves when rooms are unoccupied. Thus, additional assumptions should be considered in order to reduce the number of erroneous ACH values if no occupancy sensors are used. Moreover, in the case of rooms coupled with other rooms, it should be considered that any CO₂ decrease may be related to air coupling and mixing between rooms rather than to ventilation.

The proposed analytical approach is divided into three steps, as illustrated in Fig. 6.

First, CO₂ concentration decay curves are detected via gradient filtering, whereby only negative gradients are selected. These are represented as red lines in Fig. 6b. Second, only those decay sections with a starting point above 1000 ppm, and a slope limit (in ppm/h) are considered to obtain ACH values with almost empty indoor environments in most cases (Fig. 6c). In the monitored case studies, this slope limit is defined as −100 ppm/h, but it should be adapted according to the building use. Finally, by applying the selected CO₂ decay curves (Fig. 6d), ACH values are calculated per scenario using Eq. (9).

Once all ACH rates are calculated according to the available CO₂ decay curves, the mean value of ACHs, the number (N) of available data points, and the standard deviation (SD) are obtained per thermal stage, in accordance with Table 3. ACH values (h^{−1}) obtained during positive ventilation load (+ $Q_{\text{ven+inf}_i}$) in Stages 1 and 2 show the intensity of heat gains related to ventilation and infiltration; ACH rates (h^{−1}) during negative ventilation load (− $Q_{\text{ven+inf}_i}$) in Stages 3 and 4 characterise the intensity of ventilative cooling.

2.2.4. Key performance indicators to characterise the passive performance of buildings

The results of these three analytical approaches towards auditing the passive performance of the built environment provide various measurable indicators that characterise the thermal balance of buildings using long-term monitored data. As a result, each indoor environment (or case study) can be characterised in accordance with Table 4, which summarises the final outputs obtained through the proposed set of diagnostic analytics.

3. Results

The new analytical framework for the determination of specific heat vulnerabilities and passive cooling opportunities in the built environment was tested and validated in three well-characterised residential buildings using IoT-based monitoring data. The input data is described in Section 3.1, and the results of the analytical approach are displayed and discussed in Section 3.2.

3.1. Descriptive analysis of data

The daily profiles of indoor monitored data in the three case studies are illustrated in Fig. 7. This figure shows the overlapped daily profiles generated for temperature (1), relative humidity (2), and CO₂ concentrations (3) per indoor scenario. Daily profiles cover the monitored period, from 01 June 2021 to 31 August 2021.

Home 1 is the only scenario with AC (Fig. 7a₁₋₃). This monitored space has a split AC unit mainly used at night. It can be identified in Fig. 7-a₁ and 7-a₂ due to its lower temperature and higher relative humidity from 0:00 to 7:00. Furthermore, since the installation of this split air-conditioner was not installed with an appropriate ventilation system, this case shows the highest maximum CO₂ concentration, with values ranging between 1500 ppm and 3000 ppm at night (Fig. 7a₃).

Home 2 is located in the city centre on the top floor of a multi-family building (Fig. 7b₁₋₃). The monitored space was naturally ventilated in a closed mid-rise urban setting and without AC. This case has ceiling fans. Temperatures registered higher values than in other scenarios, with CO₂ concentrations lower than 1000 ppm most nights (Fig. 7b₃).

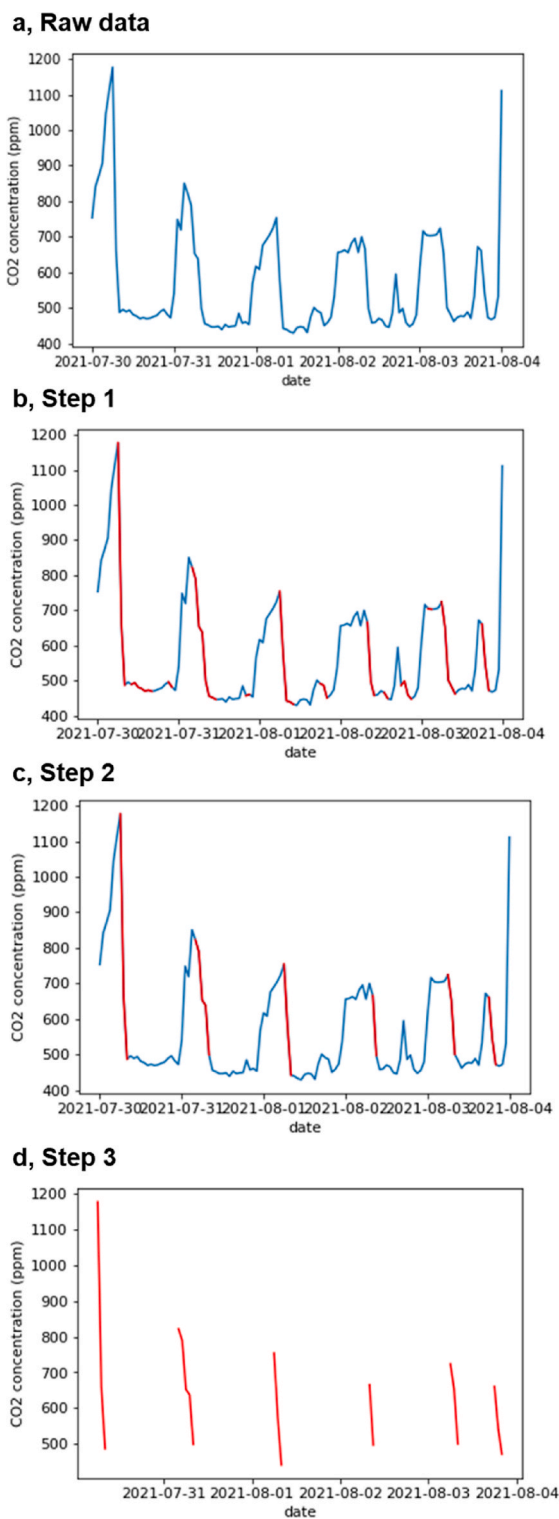


Fig. 6. Analytical steps to obtain ACHs using the CO₂-based decay method.

Home 3 has the best results from the point of view of comfort and air quality (Fig. 7c₁₋₃). This home is located on an intermediate floor of a multi-family building, and it was naturally well-ventilated with reduced heat gains. The temperature recorded the lowest values, with CO₂ concentrations below 700 ppm most nights (Fig. 7c₃).

The daily evolution of maximum and minimum temperatures for indoor and outdoor conditions throughout the monitored period is

Table 3

Summary of indicators provided by the CO₂-based ventilation analysis. Each building thermal stage is characterised by the mean ACH rate, available data points (N), and standard deviation (SD).

	Negative total heat flux ($-Q_{ti}$)	Positive total heat flux ($+Q_{ti}$)
$+Q_{ven+inf_i}$ (Mostly daytime)	ACH in Stage 1 (h^{-1}) (N; SD)	ACH in Stage 2 (h^{-1}) (N; SD)
$-Q_{ven+inf_i}$ (Mostly night-time)	ACH in Stage 4 (h^{-1}) (N; SD)	ACH in Stage 3 (h^{-1}) (N; SD)

Table 4

Summary of indicators calculated to audit the passive performance of buildings using real monitoring data.

Case study	Name	
Overheating situation	SBOI, %	
Building performance per thermal stage		
Heat fluxes		
$+Q_{ven+inf_i}$ (Mostly daytime)	Negative total heat flux ($-Q_{ti}$) Percentage of time in Stage 1 (%) ACH in Stage 1 (h^{-1}) (N; SD)	Positive total heat flux ($+Q_{ti}$) Percentage of time in Stage 1 (%) ACH in Stage 2 (h^{-1}) (N; SD)
$-Q_{ven+inf_i}$ (Mostly night-time)	Percentage of time in Stage 1 (%) ACH in Stage 4 (h^{-1}) (N; SD)	Percentage of time in Stage 1 (%) ACH in Stage 3 (h^{-1}) (N; SD)

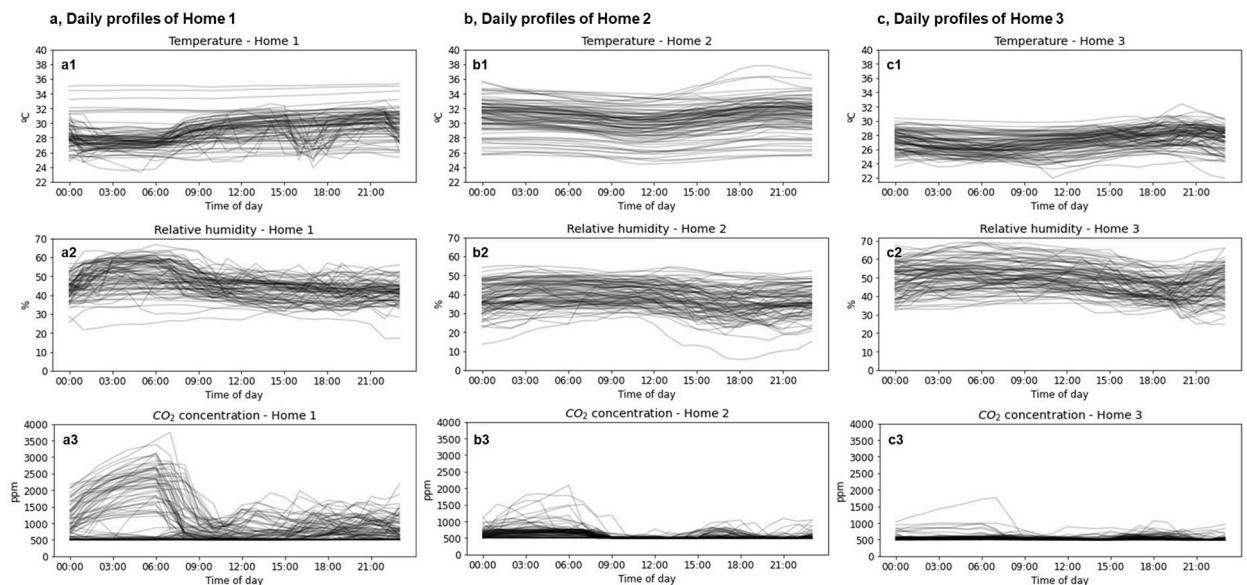


Fig. 7. Daily profiles of indoor monitored datasets for temperature, relative humidity, and CO₂ concentrations. Home 1 (a1-3), Home 2 (b1-3), and Home 3 (c1-3).

illustrated in Fig. 8, which provides a more detailed explanation of the performance of each indoor and outdoor dataset.

The comparison of outdoor temperatures between rural weather stations (WMO 083910 and WMO 083900) with an urban climate shows major differences, especially at night. Urban temperatures have maximum daytime temperatures higher than those of the rural climate by a mean value of 1 °C and by over 2 °C for peak days. Furthermore, minimum night temperatures in the urban environment are higher by a mean value of 3.5 °C compared to rural data, with some peak nights in excess of 6 °C higher. These results are similar to previous studies in the region [9].

Regarding indoor temperature values found in three homes, Fig. 8 clearly shows significant differences for discussion. As for maximum temperatures, Homes 1 and 2, located on the top floors, follow a trend with indoor temperatures much higher than those presented by Home 3, located on an intermediate floor. Homes 1 and 2 are exposed to a more vulnerable situation due to a larger transmission heat transfer surface from the roof, which increases the mean maximum temperatures by 1.75 °C and 6 °C in comparison with Home 3. Peak maximum temperature differences of Homes 1 and 2 compared to Home 3 are 3 °C and 8 °C, respectively. Additionally, regarding minimum daily temperatures, Home 3 presents lower temperature values than in other cases, thereby demonstrating its high passive cooling capacity. This appears to be directly associated with its reduced heat gains and high ventilative

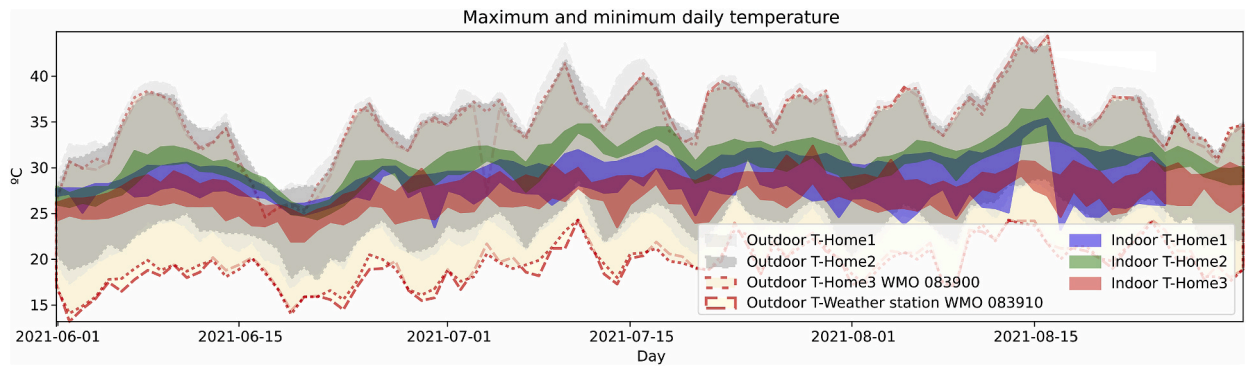


Fig. 8. The maximum and minimum daily temperature for indoor and outdoor conditions throughout the summer season.

cooling potential, which is highly influenced by its urban location, unaffected by the urban heat island. In the case of Home 1, the low minimum temperature values are due to the night-time AC use.

3.2. Analysis of the indoor passive performance of case studies through data analytics

The following sections show and discuss the results obtained by each analytic approach separately in order to validate their applicability. The final results per case study are summarised in [Appendix A](#).

3.2.1. Results of the overheating situation in case studies

The overheating situation of case studies is evaluated using the seasonal building overheating index (SBOI, %), which ranges from 0 to 100%, whereby 0% is attained for a well-designed passive building, and 100% is given for a tremendously overheated scenario with indoor temperature consistently higher than that outside. [Table 5](#) summarises the SBOI obtained per scenario.

The results show how Homes 1 and 3 have reasonably good thermal performance with an SBOI value close to 0%, ranging between 1.62 and 3.94%. It should be clarified that the SBOI value obtained in Home 1 is not valid since it is highly influenced by the operation of its AC system. In contrast, Home 2 is clearly overheated, with an SBOI value of 35.56%.

3.2.2. Results of building thermal stages

Once the overheating baselines are characterised, the analysis of building thermal stages makes it possible to determine specific heat vulnerabilities and passive cooling opportunities per building scenario using IoT-based monitoring data.

[Fig. 9](#) illustrates the heat balance map for each case study, which divides building performance into four thermal stages (or quadrants) according to the positive or negative influence of the total heat flux (Q_t), and to the ventilation and infiltration load ($Q_{ven+inf}$).

The results of the heat balance map for each scenario highlight the following findings for each building thermal stage:

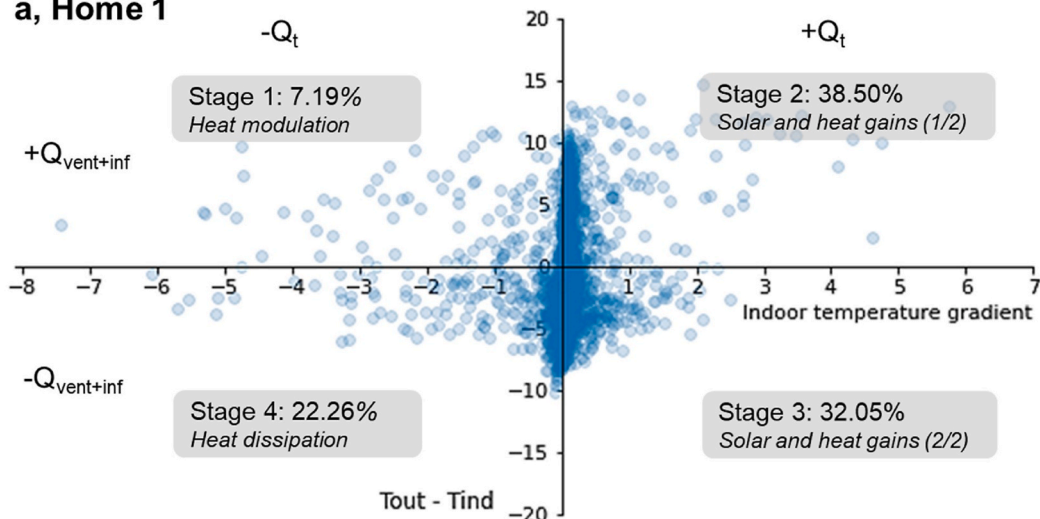
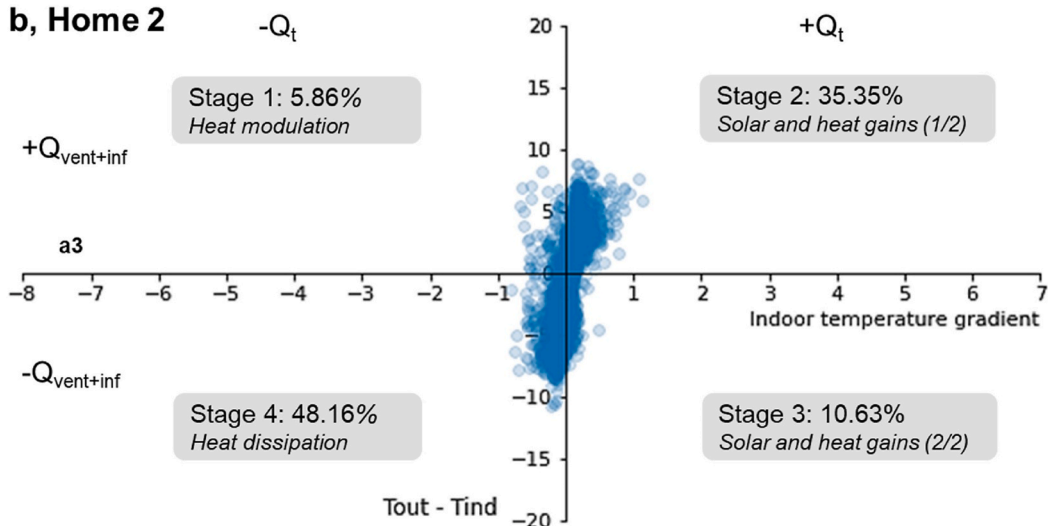
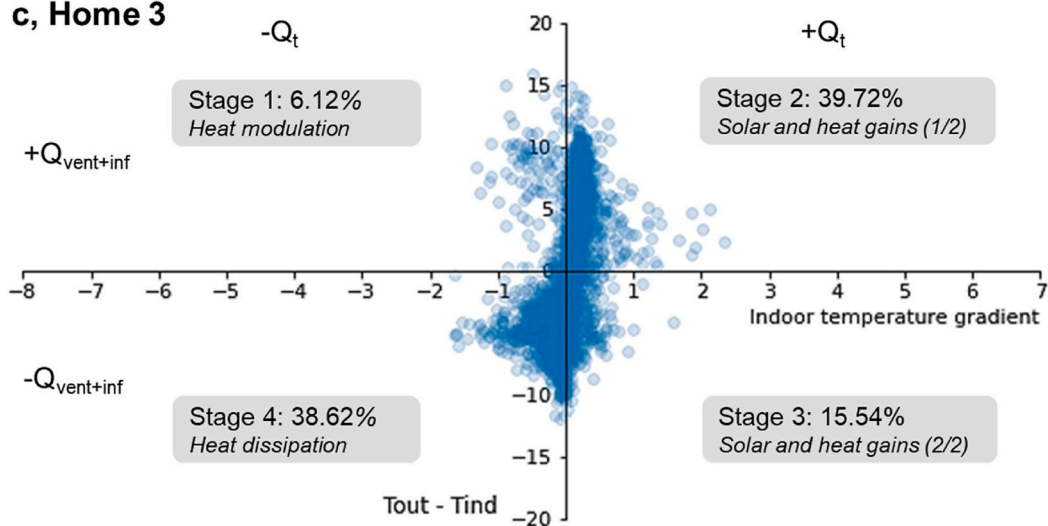
- Stage 1, in the upper left-hand quadrant, illustrates the period of the building where it is cooling despite the higher outdoor temperature ($-Q_t$ and $+Q_{ven+inf}$). This effect is mainly associated with thermal inertia or heat modulation due to building thermal mass (or active AC systems in the case of Home 1). All scenarios show a similar period in this stage, and range between 5 and 7%.
- Stage 2, in the upper right-hand quadrant, shows the building heating up with a higher outside temperature ($+Q_t$ and $+Q_{ven+inf}$). This period ranges between 35 and 40% in the monitored cases.
- Stage 3, in the lower right-hand quadrant, illustrates the period of the building where the indoor environment is heating up even with a lower outside temperature ($+Q_t$ and $-Q_{ven+inf}$). This stage presents major differences between the scenarios, with a percentage of 32% for Home 1, 11% for Home 2, and 16% for Home 3. These results highlight the lack of ventilation in Home 1 compared to Homes 2 and 3.
- Stage 4, in the lower left-hand quadrant, represents the period of the building with a negative temperature gradient and an indoor temperature higher than that outside ($-Q_t$ and $-Q_{ven+inf}$). This stage illustrates the existing heat dissipation periods via ventilation (or even active cooling periods when high negative values are provided, such as in Home 1). The results again present major differences between the cases, with a percentage of 22%, 48%, and 39% for Homes 1, 2, and 3, respectively. It should be borne in mind that Homes 2 and 3 take advantage of night ventilative cooling to cool the indoor environment, while Home 1 appears to be inadequately ventilated.

Table 5

Results of the seasonal building overheating index (SBOI, %) per scenario.

Overheating situation	Home 1	Home 2	Home 3
SBOI (%)	1.62% (invalid value ^a)	35.59%	3.99%

^a SBOI obtained for Home 1 is not valid since it is highly influenced by the operation of the AC system.

a, Home 1**b, Home 2****c, Home 3**

(caption on next page)

Fig. 9. Heat balance map per case study obtained through the analysis of building thermal stages. Stage 1: heat modulation; Stage 2: solar and heat gains (1/2); Stage 3: solar and heat gains (2/2); Stage 4: heat dissipation.

These findings, along with the overheating index previously shown, enable heat vulnerabilities to be identified in monitored cases and specific actions to be identified for the improvement of passive building performance as follows:

- In Home 1, ventilative cooling is identified as an excellent opportunity to improve passive building performance and decrease cooling demand. Home 1 has only 22% of the time in Stage 4 associated with ventilative cooling, while other cases range between 39% and 48%. The applicability of this approach for this scenario, however, has certain limitations. It should be remarked that Home 1 has an invalid overheating index due to the AC system operation, and the low percentage of time in Stage 4 may be directly related to the heating periods inside the set-point temperature band during AC operation.
- Home 2 has the highest heat vulnerability, with an SBOI of 35.59%. The heat balance map shows that this indoor environment is well-ventilated, with 48% in Stage 4. This indicates that heat gains cannot be released by ventilative cooling. In order to reduce solar and heat gains, further actions to improve the building envelope are required.
- Home 3 shows the best performance of all the cases under study. With an overheating index of 3.99% and without AC, this scenario shows a well-designed passive environment, well-ventilated at night, with a percentage of time in Stage 4 of 39%.

A summary of the indoor temperature data and the gradient analysis for the three homes are provided in Fig. 10a and b. The filled-in areas represent the data distribution. Horizontal lines indicate the median, maximum, and minimum values.

Fig. 10a confirms the warmer situation of Home 2 compared to Homes 1 and 3. Home 2 presents the highest median and maximum temperatures of 30.7 °C and 37.8 °C, respectively, during the monitored period. This is directly associated with the poorly insulated conditions without AC. On the other hand, Home 3 shows the lowest median and maximum values of 27.2 and 32.3 °C, respectively, and reaches the lowest minimum temperature, thereby confirming its good design conditions that follow the current building code. It should be noted that data distribution in Home 1 is influenced by AC operation at night.

In Fig. 10b, it can be identified how the high thermal gradient of up to ± 6 °C/h of Home 1 is associated with the active AC system, and the moderate cooling gradient in Home 3 of up to ± 2 °C/h is associated with the use of ventilative cooling. Home 2 presents the smallest gradient values of up to ± 1 °C/h due to its difficulty in modifying the internal temperature. The importance of the location of each indoor environment should also be borne in mind, since it may affect the ventilative cooling gradient due to the urban overheating effect [38], as illustrated and discussed in Fig. 8. Following this argument, Home 3 is located in a more favourable location unaffected by the urban heat island, with lower outdoor temperatures than those of Homes 1 and 2. This cooler location increases the cooling gradient in Home 3 by night ventilation due to a more significant difference in temperatures outside and inside ($T_{out_i} - T_{ind_i}$).

3.2.3. Characterisation of ventilation and infiltration rates through the CO₂-based ventilation analysis

This section evaluates the ventilation and infiltration rates per building thermal stage using the CO₂-based decay method, which calculates the real air change rates (ACH, h⁻¹) related to ventilation and infiltration for each stage. These results identify opportunities for improvement in the passive building performance concerning ventilation and infiltration rates that influence the ventilative cooling and infiltration heat load intensity.

Tables 6–8 summarise the ACH results obtained for each building performance stage in each case study. They also provide the number of values obtained in each stage (N) and the standard deviation (SD).

The analysis of ventilation and infiltration rates per thermal stage reveals the following findings for each case study.

- Home 1 and Home 2 show similar ACH for ventilative cooling at night (Stage 4), with a mean value of 0.65–0.69 h⁻¹. However, in Stage 2, when ventilation and infiltration heat flux is positive, Home 2 has a higher ACH of 1.07 h⁻¹ while Home 1 has 0.31 h⁻¹. This suggests that reducing the ACH in Stage 2 of Home 2 may positively reduce heat gains, thereby mitigating overheating. However, it should also be noted that this assumption is weak since only one ACH value was obtained at this stage in this scenario.

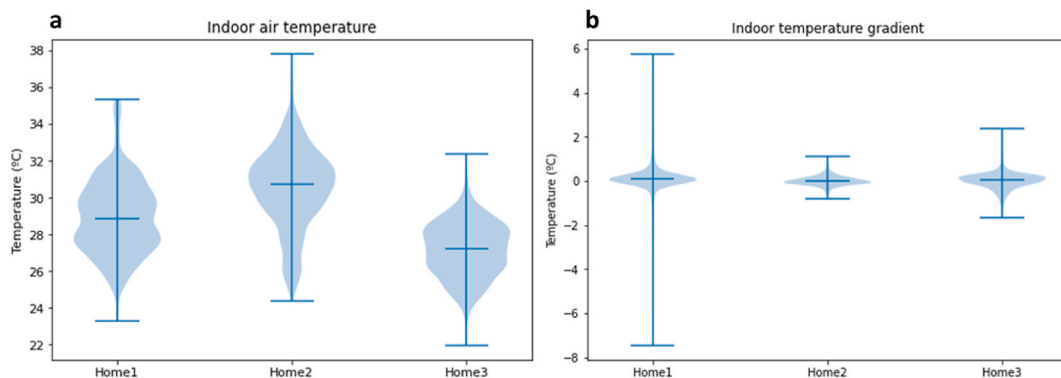


Fig. 10. Violin plot of (a) the indoor temperature, and (b) the indoor temperature gradient of the homes.

Table 6

Results of ACH rates per building performance stage in Home 1.

Heat fluxes	Negative total heat flux ($-Q_{ti}$)	Positive total heat flux ($+Q_{ti}$)
$+Q_{ven+inf_i}$ (Mostly daytime)	ACH = 0.48 h^{-1} (N: 3; SD: ± 0.23)	ACH = 0.31 h^{-1} (N: 69; SD: ± 0.03)
$-Q_{ven+inf_i}$ (Mostly night-time)	ACH = 0.69 h^{-1} (N: 14; SD: ± 0.16)	ACH = 0.64 h^{-1} (N: 108; SD: ± 0.05)

ACH: air change rates (h^{-1}), N: number of data points, SD: standard deviation (h^{-1}).**Table 7**

Results of ACH rates per building performance stage in Home 2.

Heat fluxes	Negative total heat flux ($-Q_{ti}$)	Positive total heat flux ($+Q_{ti}$)
$+Q_{ven+inf_i}$ (Mostly daytime)	ACH = - (-)	ACH = 1.07 h^{-1} (N: 1; SD: -)
$-Q_{ven+inf_i}$ (Mostly night-time)	ACH = 0.65 h^{-1} (N: 15; SD: ± 0.14)	ACH = 0.55 h^{-1} (N: 4; SD: ± 0.19)

ACH: air change rates (h^{-1}), N: number of data points, SD: standard deviation (h^{-1}).**Table 8**

Results of ACH rates per building performance stage in Home 3.

Heat fluxes	Negative total heat flux ($-Q_{ti}$)	Positive total heat flux ($+Q_{ti}$)
$+Q_{ven+inf_i}$ (Mostly daytime)	ACH = - (-)	ACH = 1.14 h^{-1} (N: 1; SD: -)
$-Q_{ven+inf_i}$ (Mostly night-time)	ACH = 1.31 h^{-1} (N: 2; SD: ± 0.72)	ACH = - (-)

ACH: air change rates (h^{-1}), N: number of data points, SD: standard deviation (h^{-1}).

- In the case of Home 3, higher ACH values were found for ventilative cooling in Stage 4 compared to the other cases. This may indicate the favourable natural ventilation design of the building through cross ventilation using an inner courtyard.

Fig. 11 summarises the results obtained per scenario. It illustrates the data distribution of CO_2 concentration (Fig. 11a) and related ACHs calculated following the CO_2 -based ventilation analysis (Fig. 11b). Horizontal lines indicate the median, maximum, and minimum values.

The results of Fig. 11a show how the CO_2 values in Home 1 are much higher than those found in the other cases, with a median of 704 ppm and peak values of 3754 ppm, way beyond the recommended thresholds [39]. On the other hand, Homes 2 and 3 have similar values, and show a median of 500 ppm and peak values of 2090 and 1760 ppm, respectively. Moreover, the data distribution of Home 3 is much lower than Home 2.

The data distribution of CO_2 concentrations is directly related to the ventilation rate achieved in each home in Fig. 11b. Home 1 presents the lowest median ACH value of 0.37 h^{-1} , which implies poor ventilation that causes the level of CO_2 to decrease more slowly. Furthermore, this case shows the most dispersed ACH values with a maximum of 2.58 h^{-1} . Home 2 shows a higher median of 0.45 h^{-1} and a greater distribution of values, ranging up to 1.91 h^{-1} . These results confirm the previous findings of a well-ventilated scenario in this indoor environment. Finally, Home 3 presents the highest ACH values, with a median of 1.14 h^{-1} , ranging from 1.25 h^{-1} to 2.03 h^{-1} .

An additional limitation of this ACH analysis is related to the appropriate CO_2 decay data required for the calculation of ACH. With well-addressed ventilation, where indoor CO_2 concentrations are low and homogeneous throughout the day, very few ACH values can be obtained using this method. Table 9 summarises the number of ACH values obtained per case study, and Fig. 12 illustrates an example of the analytical frame for each scenario.

Home 1 presents the highest number of ACH values with 195 data points thanks to its high concentrations of CO_2 . This can be

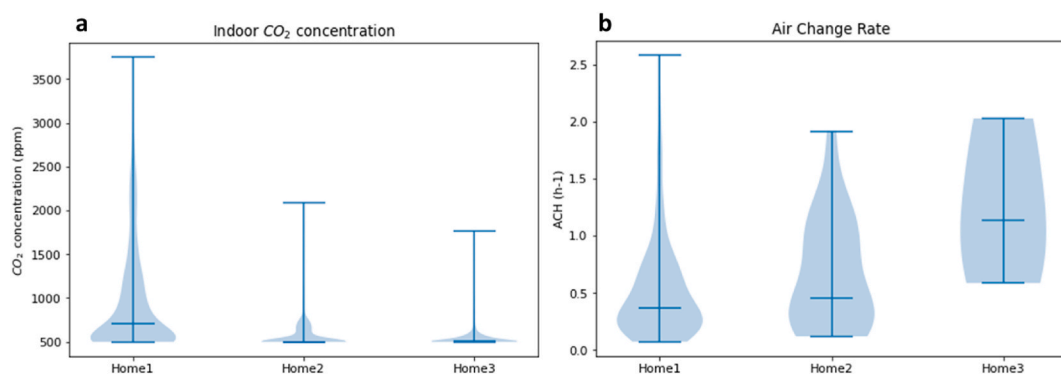
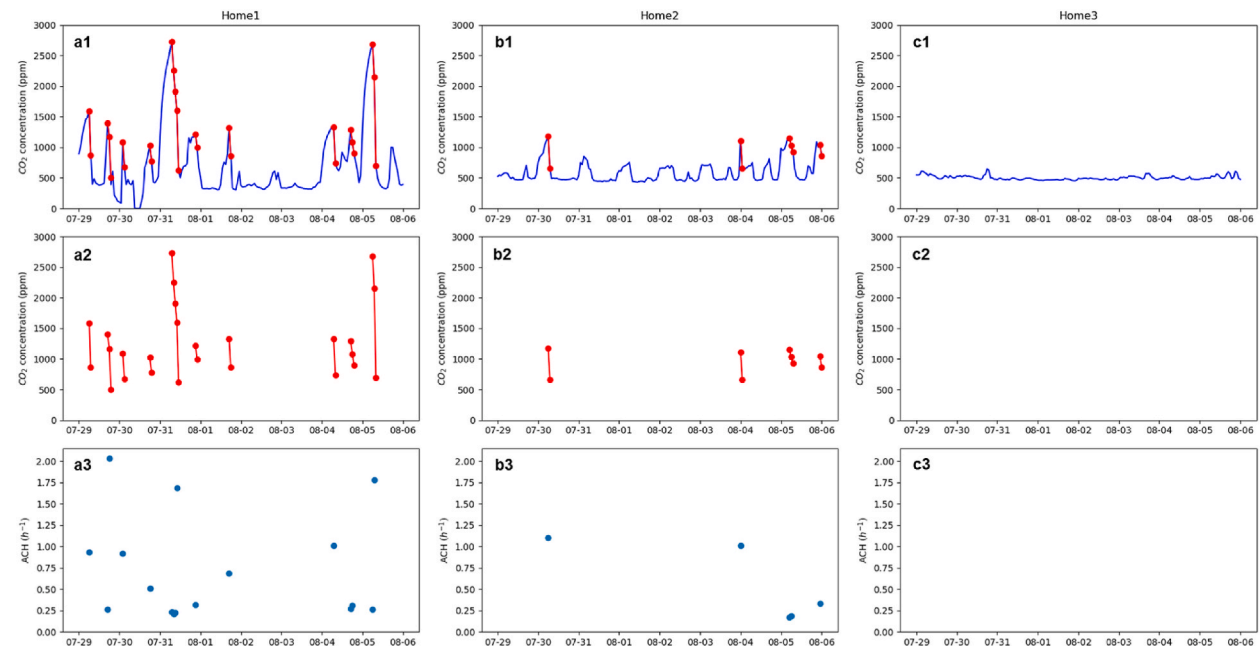
**Fig. 11.** Violin plot of (a) indoor CO_2 concentrations and (b) ACH obtained using the CO_2 -based decay method.

Table 9Summary of ACH values calculated per case study concerning hourly CO₂ data points.

	Home 1	Home 2	Home 3
Total CO ₂ data	1900 (100%)	2026 (100%)	2111 (100%)
CO ₂ decay data	194 (10.21%)	20 (0.99%)	3 (0.14%)

**Fig. 12.** Example of the analytic process using the CO₂-based decay method to obtain the ACH values per case study.

observed in Fig. 12a, where many CO₂ decay curves (red lines) are available every day for the evaluation of ACH. Home 2 shows lower availability of CO₂ decay curves that meet the criteria for calculating ACH, although it was possible to obtain 20 values to characterise the ventilation and infiltration rate. Home 3 shows an extreme case where only 3 ACH values were obtained during the monitored period since CO₂ concentrations almost always remain below 1000 ppm.

4. Discussion

The proposed set of analytics and indicators has been shown to be useful in the audit and characterisation of the passive performance of buildings using IoT-based monitoring data and in support of effective retrofitting to mitigate indoor overheating. The proposed analytical methods evaluated the overheating situation per case study, characterised building thermal stages through a heat balance map (in terms of intensity and time period), and evaluated ACH rates per thermal stage using the CO₂-based decay method.

The analytical workflow presented specific heat vulnerabilities in the building stock and supported the decision-making process towards the improvement of the building performance concerning measures based on ventilation habits, infiltration load, and/or thermal properties of the building envelope. The main findings identified in the sample under evaluation with this analytical approach are discussed below. They are grouped into the three main actions for the passive conditioning of buildings [30,31]: heat modulation, solar and heat gains, and heat dissipation.

Concerning heat modulation (in Thermal stage 1), it was shown that:

- **Building heat capacity (or thermal inertia).** No differences were found in Stage 1 in the sample under study, mainly characterised by the heat storage capacity of the buildings. In this case, the location of the insulation on the external or internal layer of the building façade may provide a different thermal performance for this stage. However, further studies are required for this to be confirmed.

Regarding solar and heat gains (in Thermal stages 2 and 3), it was found that:

- **Building storey.** Homes 1 and 2, located on the top floor of their buildings, have the higher maximum temperatures and heat vulnerability compared to Home 3, which is located on an intermediate floor. This characteristic bears a considerable influence on total solar heat gains and the surface of heat transfer with the outdoor environment, and increases the overheating of the buildings.
- **Detached, semi-detached, or terraced houses.** Home 2 is also characterised as a semi-detached multi-family building, with a greater external building envelope surface than have Homes 1 and 3, thereby further increasing associated heat gains.

- **Insulation level.** The selected case studies differ in terms of their U-values according to different thermal regulations. The results suggested that Homes 1 and 3 present a better performance due to their higher insulation standard.
- **Infiltration heat gains.** The ACH values calculated in Thermal stage 2 show the heat load associated with infiltration. The results highlighted the low infiltration heat rate in Home 1 of 0.31 h^{-1} , mainly related to the characteristics of the new double-glazed windows, but they also negatively affect indoor CO_2 concentrations. On the other hand, higher ACH values associated with infiltration heat gains were found in Homes 2 and 3, ranging between 1.07 h^{-1} and 1.14 h^{-1} . These higher values may indicate a good opportunity to reduce heat gains by decreasing infiltration. However, additional data should be collected to confirm this hypothesis due to the low number of valid ACH values.

Finally, the most important passive cooling strategy is that of natural ventilation in terms of heat dissipation (Thermal stage 4). From the analysis, it can be highlighted that:

- **Building location affected by urban or rural climate.** The intensity of ventilative cooling in Stage 4 (Fig. 9) was higher in Home 3 than in the other dwellings. This may largely be related to the fact that Home 3 is located in a suburban area of the city, unaffected by the urban heat island. Moreover, suburban areas do not present urban obstacles that would otherwise reduce the wind speed against the façade of the building.
- **Building orientation, and single-sided or cross ventilation.** A higher mean ACH of 1.31 h^{-1} for night ventilation in Stage 4 was found in Home 3 compared to Homes 1 and 2, characterised by an ACH of $0.65\text{--}0.69 \text{ h}^{-1}$. This fact can be directly related to two specific configurations of Home 3 that are not present in the other homes: cross-ventilation through an inner courtyard and the building façade facing prevailing winds during the monitored period, according to the seasonal wind rose provided in Fig. 13. The poor ACH values of Home 1 may be related to inadequate design (orientation and single-sided ventilation). The east-facing orientation combined with single-sided ventilation does not favour the ventilation of the space since the wind is predominantly from the southwest. Therefore, additional effort may be required to increase ACHs and improve indoor conditions of air quality.
- **Type of AC system:** Higher CO_2 concentrations were found in Home 1 due to the operation of the AC system without adequate ventilation. This fact constrained the opportunity for free cooling using night ventilation. Home 1 shows a low ventilative cooling period of 22% in Stage 4, while Homes 2 and 3 range between 39% and 48%.

The results supported the identification of indoor environments with ventilative cooling opportunities to decrease the indoor temperature, such as that of Home 1. Moreover, they highlighted those scenarios in which additional solutions to mitigate solar and heat gains should be implemented to improve building performance, such as Home 2. Furthermore, it was demonstrated how ventilative cooling potential is highly influenced by the effect of the location of the building (urban heat island), orientation (prevailing winds), and by whether it has single-sided or cross ventilation. These three aspects constitute the main reason for the better passive thermal performance in Home 3, which is well-oriented, enjoys cross ventilation, and is exposed to a suburban climate. Finally, the potential application of this analytical approach should be considered on a larger scale (in a large sample of buildings). This approach can statistically identify specific characteristics, designs, and/or configurations that would provide worse or better performance across the sample. This large-scale application could facilitate the identification of particular building configurations that should be either limited or promoted in future building codes and guidelines.

5. Conclusions

This research proposes innovative diagnostic analytics to audit the passive performance of buildings using long-term monitoring data. The aim is to quantify heat vulnerabilities and identify optimal passive cooling alternatives in order to retrofit the built environment through a swift and less-disruptive evaluation of the real performance of buildings. Three analytical methods have been developed in Python code that provide: a novel seasonal overheating index (SBOI) ranging from 0 to 100%; a heat balance

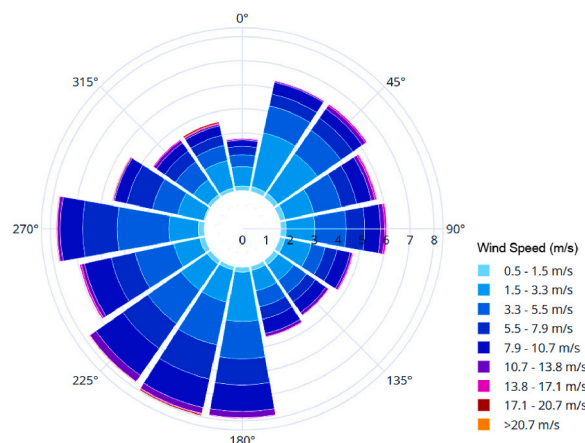


Fig. 13. Seasonal wind rose using data for weather station WMO 083900. Observations from June to August.

map that characterises building performance into four thermal stages related to the positive or negative influence of total heat flux, together with the ventilation and infiltration load; and the mean air change rates (ACH, h^{-1}) per thermal stage using the CO_2 -based decay method. The proposed methods have been tested, discussed, and validated using IoT-based monitoring data in three residential case studies in southern Europe, monitored from June to August 2021. Based on the results, the following conclusions can be drawn:

The results demonstrate how the proposed diagnostic analytics using monitoring data quickly characterise the overheating situation of each case study and identify passive cooling opportunities with regard to existing solar and heat gains, available heat dissipation, and heat modulation techniques. The indicators highlight the good passive performance of Home 3 (SBOI = 3.99%) and the more vulnerable scenario of Home 2 (SBOI = 35.59%). Moreover, the analysis identifies the best available passive cooling opportunities. Ventilative cooling was found to mitigate indoor overheating in Home 1, with a potential increase from 22% to 48% of the time; and reducing solar and heat gains were found to be the best alternative in Home 2 since it already showed a high ventilative cooling profile of 48% of the time. Additionally, the characterisation of the ACH rates through the CO_2 -based decay method was able to quantify the mean ventilative cooling rate at night, and the mean infiltration rate increasing heat gains in the daytime. The results identified how reducing the ACH of 1.07 h^{-1} associated with infiltration heat gains in Home 2 may positively impact indoor temperature.

Additionally, in large-scale applications and with additional metadata of buildings, this approach could also statistically identify specific building designs, characteristics, and/or operating conditions that provide worse or better passive performance extended across the sample. Its potential usefulness includes a large-scale application to support designers in the identification of particular building characteristics that should either be limited or promoted in future building codes in order to mitigate the impact of heat in the built environment.

As practical insights, this study highlights how diagnostic analytics using real monitoring data can play a major role in auditing and characterising seasonal building performance beyond the standard or normalised tests, and can efficiently support building retrofitting. Future studies will implement additional IoT monitoring sensors, such as occupancy sensors and window-opening sensors, to improve the accuracy of reported indicators. Additionally, different locations, building designs, configurations, and operating conditions will be tested to define guideline thresholds of a more accurate nature to support passive building design. The source code of these diagnostic methods is published under the MIT licence on GitHub (<https://github.com/lizanafj/analytics-to-assess-the-heat-resilience-of-buildings>) together with the relevant documentation and tutorials.

Author statement

Elisa López-García: Conceptualization, Methodology, Data curation, Investigation, Software, Formal analysis, Visualization, Validation, Writing - Original draft, Writing - Review & Editing. **Jesús Lizana:** Conceptualization, Methodology, Data curation, Investigation, Formal analysis, Visualization, Validation, Supervision, Writing - Original draft, Writing - Review & Editing. **Antonio Serrano-Jiménez** (Corresponding author): Conceptualization, Methodology, Data Curation, Investigation, Formal analysis, Visualization, Validation, Supervision, Writing - Review & Editing. **Carmen Díaz-López:** Methodology, Investigation, Validation, Formal analysis, Supervision, Writing - Review & Editing. **Ángela Barrios-Padura:** Conceptualization, Investigation, Funding acquisition, Project Administration, Supervision.

Declaration of competing interest

The authors declare that they have no known competing financial interests or personal relationships that could have appeared to influence the work reported in this paper.

Acknowledgements

This work has been supported through funds, materials, and measuring equipment as part of the “Eco-efficiency in educational centres: Innovation, Rehabilitation and regeneration” research project (US-15547), within the ERDF for the Andalusian region 2014–2020, and the “(Re)programa-tool: Digital tool for optimised decision-making in housing renovation strategies” (Andalusian Government – US.20-06). The research was also funded by the European Union’s Horizon 2020 research and innovation programme under the Marie Skłodowska-Curie grant agreement No 101023241. This research received financial support from the Andalusian Government (Junta de Andalucía-Consejería de Economía, Innovación y Ciencia) through a postdoctoral contract POST-DOC_21-00575 granted to Antonio Serrano-Jiménez; it was also funded by the Spanish Ministry of Universities with Next-Generation Funds from the European Union through the Margarita Salas postdoctoral contract granted to Carmen Díaz-López. Finally, the authors would also like to thank AEMET (State Meteorological Agency of Spain) for the weather data provided for this research, and Lesley Burrige for the English proofreading.

Appendix A. Summary of results obtained per case study

Tables A1-A3 summarise the results of all indicators obtained through this analytical framework to audit the passive performance of buildings.

Table A1

Results of indicators to characterise the passive performance of Home 1.

Case study	Home 1	
Overheating index	SBOI = 1.62% (invalid value ^a)	
Building performance per thermal stage		
Heat fluxes	Negative total heat flux (− Q _{ti})	Positive total heat flux (+ Q _{ti})
+Q _{ven+inf_i} (Mostly daytime)	Thermal stage 1 Percentage of time = 7.19% ACH = 0.48 h ^{−1} (N: 3; SD: ±0.23)	Thermal stage 2 Percentage of time = 38.50% ACH = 0.31 h ^{−1} (N: 69; SD: ±0.03)
−Q _{ven+inf_i} (Mostly night-time)	Thermal stage 4 Percentage of time = 22.26% ACH = 0.69 h ^{−1} (N: 14; SD: ±0.16)	Thermal stage 3 Percentage of time = 32.05% ACH = 0.64 h ^{−1} (N: 108; SD: ±0.05)

^a SBOI obtained for Home 1 is not valid since it is highly influenced by the operation of the AC system.**Table A2**

Results of indicators to characterise the passive performance of Home 2.

Case study	Home 2	
Overheating index	SBOI = 35.59%	
Building performance per thermal stage		
Heat fluxes	Negative total heat flux (− Q _{ti})	Positive total heat flux (+ Q _{ti})
+Q _{ven+inf_i} (Mostly daytime)	Thermal stage 1 Percentage of time = 5.86% ACH = - (-)	Thermal stage 2 Percentage of time = 35.35% ACH = 1.07 h ⁻¹ (N: 1; SD:)
−Q _{ven+inf_i} (Mostly night-time)	Thermal stage 4 Percentage of time = 48.16% ACH = 0.65 h ⁻¹ (N: 15; SD: ±0.14)	Thermal stage 3 Percentage of time = 10.63% ACH = 0.55 h ⁻¹ (N: 4; SD: ±0.19)

Table A3

Results of indicators to characterise the performance of Home 3.

Case study	Home 3	
Overheating index	SBOI = 3.99%	
Building performance per thermal stage		
Heat fluxes	Negative total heat flux (− Q _{ti})	Positive total heat flux (+ Q _{ti})
+Q _{ven+inf_i} (Mostly daytime)	Thermal stage 1 Percentage of time = 6.12% ACH = - (−)	Thermal stage 2 Percentage of time = 39.72% ACH = 1.14 h ^{−1} (N: 1; SD:)
−Q _{ven+inf_i} (Mostly night-time)	Thermal stage 4 Percentage of time = 38.62% ACH = 1.31 h ^{−1} (N: 2; SD: ±0.72)	Thermal stage 3 Percentage of time = 15.54% ACH = - (−)

References

- [1] IEA, The Future of Cooling, Opportunities for Energy-Efficient Air Conditioning, IEA Publications, Paris, 2018. <https://www.iea.org/reports/the-future-of-cooling>.
- [2] IPCC, Climate Change 2022. Mitigation of Climate Change. Working Group III Contribution to the Sixth Assessment Report of the Intergovernmental Panel on Climate Change, 2022.
- [3] Z. Ma, P. Cooper, D. Daly, L. Ledo, Existing building retrofits: Methodology and state-of-the-art, Energy Build. 55 (2012) 889–902, <https://doi.org/10.1016/j.enbuild.2012.08.018>.
- [4] J. Lizana, Á. Barrios-Padura, M. Molina-Huelva, R. Chacartegui, Multi-criteria assessment for the effective decision management in residential energy retrofitting, Energy Build. 129 (2016) 284–307, <https://doi.org/10.1016/j.enbuild.2016.07.043>.
- [5] A. Grubler, C. Wilson, N. Bento, B. Boza-Kiss, V. Krey, D.L. McCollum, N.D. Rao, K. Riahi, J. Rogelj, S. De Stercke, J. Cullen, S. Frank, O. Fricko, F. Guo, M. Gidden, P. Havlík, D. Huppmann, G. Kiesewetter, P. Rafaj, W. Schoepp, H. Valin, A low energy demand scenario for meeting the 1.5 °C target and sustainable development goals without negative emission technologies, Nat. Energy 3 (2018) 515–527, <https://doi.org/10.1038/s41560-018-0172-6>.
- [6] International Energy Agency, Transition to Sustainable Buildings. Strategies and Opportunities to 2050, OECD/IEA, 2013, <https://doi.org/10.1787/9789264202955-en>.
- [7] M. Economidou, V. Todeschi, P. Bertoldi, D. D'Agostino, P. Zangheri, L. Castellazzi, Review of 50 years of EU energy efficiency policies for buildings, Energy Build. 225 (2020), 110322, <https://doi.org/10.1016/j.enbuild.2020.110322>.
- [8] H.W. Samuelson, A. Baniassadi, P.I. Gonzalez, Beyond energy savings: investigating the co-benefits of heat resilient architecture, Energy 204 (2020), 117886, <https://doi.org/10.1016/j.energy.2020.117886>.
- [9] J. Lizana, V.P. López-Cabeza, R. Renaldi, E. Diz-Mellado, C. Rivera-Gómez, C. Galán-Marín, Integrating courtyard microclimate in building performance to mitigate extreme urban heat impacts, Sustain. Cities Soc. 78 (2021), 103590, <https://doi.org/10.1016/j.scs.2021.103590>.
- [10] D. Fosas, D.A. Coley, S. Natarajan, M. Herrera, M. Fosas de Pando, A. Ramallo-Gonzalez, Mitigation versus adaptation: does insulating dwellings increase overheating risk? Build. Environ. 143 (2018) 740–759, <https://doi.org/10.1016/j.buildenv.2018.07.033>.
- [11] C. Sanchez-Guevara, M. Peiró Núñez, J. Taylor, A. Mavrogianni, J. Neila González, Assessing population vulnerability towards summer energy poverty: case studies of Madrid and London, Energy Build. 190 (2019) 132–143, <https://doi.org/10.1016/j.enbuild.2019.02.024>.

- [12] C. Zhang, O.B. Kazanci, R. Levinson, P. Heiselberg, B.W. Olesen, G. Chiesa, B. Sodagar, Z. Ai, S. Selkowitz, M. Zinzi, A. Mahdavi, H. Teufl, M. Kolokotroni, A. Salvati, E. Bozonnet, F. Chtioui, P. Salagnac, R. Rahif, S. Attia, V. Lemort, E. Elnagar, H. Breesch, A. Sengupta, L.L. Wang, D. Qi, P. Stern, N. Yoon, D.I. Bogatu, R.F. Rupp, T. Arghand, S. Javed, J. Akander, A. Hayati, M. Cehlin, S. Sayadi, S. Forghani, H. Zhang, E. Arens, G. Zhang, Resilient cooling strategies – a critical review and qualitative assessment, *Energy Build.* 251 (2021), 111312, <https://doi.org/10.1016/j.enbuild.2021.111312>.
- [13] S. Attia, R. Levinson, E. Ndongo, P. Holzer, O. Berk Kazanci, S. Homaie, C. Zhang, B.W. Olesen, D. Qi, M. Hamdy, P. Heiselberg, Resilient cooling of buildings to protect against heat waves and power outages: key concepts and definition, *Energy Build.* 239 (2021), 110869, <https://doi.org/10.1016/j.enbuild.2021.110869>.
- [14] M. Chen, S. Mao, Y. Liu, Big data: a survey, *Mobile Network. Appl.* 19 (2014) 171–209, <https://doi.org/10.1007/s11036-013-0489-0>.
- [15] K. Lawal, H.N. Rafsanjani, Trends, benefits, risks, and challenges of IoT implementation in residential and commercial buildings, *Energy Built Environ* (2021), <https://doi.org/10.1016/j.enbenv.2021.01.009>.
- [16] T. Hong, L. Yang, D. Hill, W. Feng, Data and analytics to inform energy retrofit of high performance buildings, *Appl. Energy* 126 (2014) 90–106, <https://doi.org/10.1016/j.apenergy.2014.03.052>.
- [17] M.M. Abdelrahman, S. Zhan, C. Miller, A. Chong, Data science for building energy efficiency: a comprehensive text-mining driven review of scientific literature, *Energy Build.* 242 (2021), 110885, <https://doi.org/10.1016/j.enbuild.2021.110885>.
- [18] A. Serrano-Jiménez, J. Lizana, M. Molina-Huelva, Á. Barrios-Padura, Indoor environmental quality in social housing with elderly occupants in Spain: measurement results and retrofit opportunities, *J. Build. Eng.* 30 (2020), <https://doi.org/10.1016/j.jobbe.2020.101264>.
- [19] L. Stabile, M. Dell'Isola, A. Russi, A. Massimo, G. Buonanno, The effect of natural ventilation strategy on indoor air quality in schools, *Sci. Total Environ.* 595 (2017) 894–902, <https://doi.org/10.1016/j.scitotenv.2017.03.048>.
- [20] J. Lizana, S.M. Almeida, A. Serrano-Jiménez, J.A. Becerra, M. Gil-Báez, Á. Barrios-Padura, R. Chacartegui, Contribution of indoor microenvironments to the daily inhaled dose of air pollutants in children. The importance of bedrooms, *Build. Environ.* 183 (2020), 107188, <https://doi.org/10.1016/j.buildenv.2020.107188>.
- [21] X. Sui, Z. Tian, H. Liu, H. Chen, D. Wang, Field measurements on indoor air quality of a residential building in Xi'an under different ventilation modes in winter, *J. Build. Eng.* 42 (2021), 103040, <https://doi.org/10.1016/j.jobbe.2021.103040>.
- [22] K. Huang, J. Song, G. Feng, Q. Chang, B. Jiang, J. Wang, W. Sun, H. Li, J. Wang, X. Fang, Indoor air quality analysis of residential buildings in northeast China based on field measurements and longtime monitoring, *Build. Environ.* 144 (2018) 171–183, <https://doi.org/10.1016/j.buildenv.2018.08.022>.
- [23] M. Pieš, R. Hájovský, J. Velická, Design, implementation and data analysis of an embedded system for measuring environmental quantities, *Sensors* (2020) 20, <https://doi.org/10.3390/s20082304>.
- [24] J.J. Sendra, S. Domínguez-Amarillo, P. Bustamante, A.L. León, Energy intervention in the residential sector in the south of Spain: current challenges, *Inf. La Construcción.* 65 (2013) 457–464, <https://doi.org/10.3989/ic.13.074>.
- [25] D. Waters, A. Donnellan, J. Fox, An adaptable Internet of Things network infrastructure implemented for a smart building system, 2021 32nd Irish signals syst. Conf. ISSC (2021), <https://doi.org/10.1109/ISSC52156.2021.9467837>, 2021.
- [26] P. Moura, J.I. Moreno, G.L. López, M. Alvarez-Campana, IoT platform for energy sustainability in university campuses, *Sensors* 21 (2021), <https://doi.org/10.3390/s21020357>, 1–22.
- [27] I.D. Stewart, T.R. Oke, Local climate zones for urban temperature studies, *Bull. Am. Meteorol. Soc.* 93 (2012) 1879–1900, <https://doi.org/10.1175/BAMS-D-11-00019.1>.
- [28] Government of Spain, AEMET State Meteorological Agency, (2019). <http://www.aemet.es/> (accessed September 1, 2020).
- [29] European Commission, EU Buildings Factsheets, (n.d.). https://ec.europa.eu/energy/eu-buildings-factsheets_en?redir=1.
- [30] D.K. Bhamare, M.K. Rathod, J. Banerjee, Passive cooling techniques for building and their applicability in different climatic zones—the state of art, *Energy Build.* 198 (2019) 467–490, <https://doi.org/10.1016/j.enbuild.2019.06.023>.
- [31] Y. ling Song, K.S. Darani, A.I. Khdaif, G. Abu-Rumman, R. Kalbasi, A review on conventional passive cooling methods applicable to arid and warm climates considering economic cost and efficiency analysis in resource-based cities, *Energy Rep.* 7 (2021) 2784–2820, <https://doi.org/10.1016/j.egyr.2021.04.056>.
- [32] ASHRAE Handbook - Fundamentals, SI Edition, 2017.
- [33] CIBSE, A. Guide, *Environ. Design.* (2007).
- [34] T. Gerrish, K. Ruikar, M. Cook, M. Johnson, M. Phillip, Analysis of basic building performance data for identification of performance issues, *Facilities* 35 (2017) 801–817, <https://doi.org/10.1108/F-01-2016-0003>.
- [35] V. Turanjanin, B. Vucicevic, M. Jovanovic, N. Mirkov, I. Lazovic, Indoor CO2 measurements in Serbian schools and ventilation rate calculation, *Energy* 77 (2014) 290–296, <https://doi.org/10.1016/j.energy.2014.10.028>.
- [36] Y. You, C. Niu, J. Zhou, Y. Liu, Z. Bai, J. Zhang, F. He, N. Zhang, Measurement of air exchange rates in different indoor environments using continuous CO2 sensors, *J. Environ. Sci.* 24 (2012) 657–664, [https://doi.org/10.1016/S1001-0742\(11\)60812-7](https://doi.org/10.1016/S1001-0742(11)60812-7).
- [37] S. Batterman, Review and extension of CO2-based methods to determine ventilation rates with application to school classrooms, *Int. J. Environ. Res. Publ. Health* 14 (2017) 1–22, <https://doi.org/10.3390/ijerph14020145>.
- [38] A. Serrano-Jiménez, J. Hiruelo-Pérez, E. Ramírez-Juidias, Á. Barrios-Padura, Identifying design shortcomings and heat-island effects in schools located in warm climates: an outdoor environmental assessment procedure based on remote sensing tools, *J. Build. Eng.* 43 (2021), <https://doi.org/10.1016/j.jobbe.2021.103209>.
- [39] J.A. Becerra, J. Lizana, M. Gil, Á. Barrios-Padura, P. Blondeau, R. Chacartegui, Identification of potential indoor air pollutants in schools, *J. Clean. Prod.* 242 (2020), <https://doi.org/10.1016/j.jclepro.2019.118420>.